Relative pressure estimation from velocity measurements in blood flows: state-of-the-art and new approaches

Cristobal Bertoglio, Rodolfo Núñez, Felipe Galarce, David Nordsletten, Axel Osses

Relative pressure estimation from velocity measurements in blood flows: state-of-the-art and new approaches

Cristóbal Bertoglio[1], Rodolfo Núñez[1], Felipe Galarce[1,2], David Nordsletten[3], and Axel Osses[1]

[1]Center for Mathematical Modeling, Universidad de Chile, Chile
[2]Civil Engineering School, P. Universidad Católica de Valparaiso, Chile
[3]Department of Biomedical Engineering, King's College of London, UK

June 15, 2016

Abstract

The pressure gradient across stenotic blood vessels is an important clinical index for the diagnosis of many cardiovascular diseases. While clinical gold standard for its measurement (in terms of accuracy) is invasive catheterization, Phase-Contrast MR-imaging has emerged as a promising tool for enabling a non-invasive quantification, by linking (highly spatially resolved) velocity measurements with relative pressures via Navier-Stokes equations. In this work we provide a review of current methods for relative pressure estimation, propose new ones and compare them on numerical examples using subsampled and noisy synthetic data. We verify that the newly proposed approaches are more robust with respect to data perturbations and therefore more precise.

1 Introduction

Pressure difference across stenotic blood vessels is a standard clinical measurement that serves to assess the severity of the pathology. It may be performed several times during diagnosis and follow up, for example, in congenital heart diseases [14]. The most reliable procedure in clinical practice to obtain pressure gradients involves invasive X-ray guided catheterization, which should be avoided unless non-invasive evaluations (like ultrasound) are inconclusive or discordant with clinical findings [12].

Alternatively, Phase-Contrast Magnetic Resonance Imaging (PC-MRI) allows to obtain three-dimensional, time-resolved measurements of velocity fields, allowing visualization of complex blood flow patterns in large vessels and the heart [9]. Typical PC-MRI spatial and temporal resolutions go from 1.5 to 3 mm^3 and $20 - 40$ ms, respectively [4].

Previous works have postulated methods to estimate relative pressures using these measured velocities and the Navier–Stokes equations. To the best of the authors knowledge, the oldest method in use is the so called Pressure Poisson Estimator (PPE), see for example [6, 5, 7]. It consists in reconstructing the relative pressure field by directly plugging the velocity measurements into the Navier–Stokes equations (NSE), and solving a Poisson equation for the pressure.

As a new approach, recently in [10] the authors proposed to perturb the Navier-Stokes residual with an auxiliary divergence-free vector, resulting in a mixed problem for this vector and the pressure to be estimated. Therefore it was denoted as Stokes Estimator (STE). In the tests presented in [10], STE turned out to outperform the PPE in terms of precision.

Also very recently in [3], relative pressure and velocity measurements were proposed to be related by using the classical integral energy balance of the incompressible Navier–Stokes equations, denoted as WERP. This has the advantage that only few integrals have to be evaluated, making it computationally faster than PPE and STE. However, the authors indicated some potential drawbacks: (i) the velocity measurement terms are squared, amplifying the noise, in particular for small in-/outflows, and (ii) it cannot be applied for simultaneous estimation of relative pressure in multiple outlet geometries. Nevertheless, WERP also outperformed PPE for peak relative pressure estimates.

The purpose of this manuscript is twofold. First, to compare the methods recently proposed (STE and WERP). Secondly, to propose improvements of such methods. For the STE, we show that a simple integration by parts of the terms containing the velocity considerably improves the robustness regarding spatial subsampling. Then, inspired from the WERP, we formulate an integral approach based on the momentum balance for estimating relative pressures. We also derived formulae of the statistical bias of all methods, what to the best of the authors knowledge has not yet been reported. We confirm numerically that all methods, with exception of the WERP, have a negligible bias.

The rest of this paper is organized as follows. In Section 2 we set up the pressure estimation problem. In Section 3 we revisit the state-of-the-art methods mentioned above. In Section 4 we propose new pressure estimation approaches. In Section 5 we perform a theoretical bias analysis for all the methods. In Section 6 we test and compare all methods using synthetic data, including sensitivity to noise, spatial and temporal subsampling. Finally in Section 7 we discuss the results and draw some conclusions and perspectives.

2 The relative pressure estimation problem

In this work we deal with the estimation of relative pressures from velocity image data, so we first detail in this section the assumptions about the flow physics and the data.

Let us consider an incompressible, Newtonian fluid in a bounded domain $\Omega \subset \mathbb{R}^d$, $d = 3$, modeled by the incompressible Navier–Stokes equations with the velocity $\boldsymbol{u}(t) : \Omega \to \mathbb{R}^d$ and

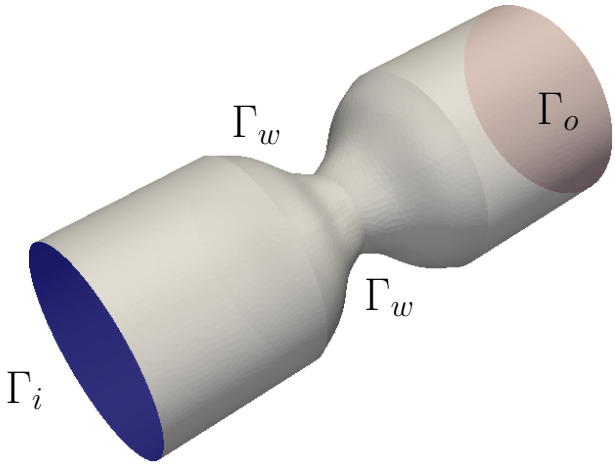

Figure 1: Stenosed geometry with 60% coarctation.

the pressure $p(t) : \Omega \to \mathbb{R}$, $t \in [0, T]$:

$$\begin{cases} \rho \partial_t \boldsymbol{u} + \rho(\boldsymbol{u} \cdot \boldsymbol{\nabla})\boldsymbol{u} - \mu \Delta \boldsymbol{u} + \boldsymbol{\nabla} p = \boldsymbol{0} & \text{in} \quad \Omega \times [0, T], \\ \boldsymbol{\nabla} \cdot \boldsymbol{u} = 0 & \text{in} \quad \Omega \times [0, T] \end{cases} \tag{1}$$

where ρ is the density and μ the dynamic viscosity. For our purposes, Ω will be the domain around the stenosis. We also assume that the boundary of Ω is given by $\partial\Omega := \Gamma = \Gamma_i \cup \Gamma_o \cup \Gamma_w$, with $\Gamma_i \cap \Gamma_o = \emptyset$. Γ_i is the inlet boundary (i.e. upstream of the obstruction), Γ_o the outlet boundary (downstream of the obstruction) and Γ_w is the arterial wall boundary, see example in Figure 1. The task of the relative pressure estimation is then to compute:

$$\delta p = \frac{1}{|\Gamma_i|} \int_{\Gamma_i} p - \frac{1}{|\Gamma_o|} \int_{\Gamma_o} p \tag{2}$$

given (perturbed) measurements of $\boldsymbol{u}$ in Ω.

As is obtained in Phase-Contrast MRI, we will assume that the velocity measurements are available at h-spaced discrete points of the domain Ω, but we will be able to reconstruct them everywhere by: (a) computing a mesh $\mathcal{T}_h$ of the domain Ω using the measurement locations and a segmented geometry from the images, and then (b) interpolating the velocity components at every point in Ω using simple linear piecewise finite element basis functions. Additionally, we will asume that these space-discrete measurements will be available at N discrete measurement times $t^1, ..., t^N$ at a constant time interval τ. We will denote the measurements as $\boldsymbol{u}_m^1, ..., \boldsymbol{u}_m^N \in [\mathcal{P}_{1,h}]^d$, with $\mathcal{P}_{1,h}$ the usual piecewise continuous linear polynomial finite element space.

Moreover, for further analysis we assume that the measurements include a random, additive perturbation with respect to the ground truth velocity, i.e. $\boldsymbol{u}_m^n = \boldsymbol{u}_h^n + \boldsymbol{\varepsilon}^n$, with $\boldsymbol{u}_h^n \in [\mathcal{P}_{1,h}]^d$ a spatial subsampling of the true field $\boldsymbol{u}$ into $[\mathcal{P}_{1,h}]^d$ at observation time t^n, and $\boldsymbol{\varepsilon}^n \in [\mathcal{P}_{1,h}]^d$ a discrete noise field, with all degrees-of-freedom independently identically distributed (i.i.d.) following a normal distribution $\mathcal{N}(0, \sigma^2)$.

Notice that we assume only the reference field $\boldsymbol{u}$ to satisfy Problem (1) (in practice we will compute one from a highly resolved numerical simulation). The discrete measured velocity fields $\boldsymbol{u}_h^n$ are the result of a subsampling operator, and therefore they do not fulfill neither (1)

nor a discretized version of it. Naturally, the same applies to $\boldsymbol{u}_m^n$ which includes additional random perturbations.

3 State of the art of estimation methods

In this section, we overview the mathematical formulations of the currently available methods to estimate relative pressure. We start with the *Poisson Pressure Estimator (PPE)*, which is the oldest and most popular. We continue with the *Stokes estimator (STE)* and then with the *Work-Energy Relative pressure estimator (WERP)*, both recently introduced. We remark that the later two approaches has been independently reported to have a superior performance than the PPE, but not have been yet compared with each other.

3.1 The Poisson Pressure Estimator (PPE)

The PPE, in the context of finite elements, is based on the assumption that the pressure gradient $\boldsymbol{\nabla} p$ satisfies a weak version of Equation (1). Hence, the estimated relative pressure at time $t^{n+1/2} := (t^n + t^{n+1})/2$ can be found as a solution of the following problem: Find $p_{\text{ppe}}^{n+1/2} \in \mathcal{P}_{1,h}$ such that

$$\int_\Omega \boldsymbol{\nabla} p_{\text{ppe}}^{n+1/2} \cdot \boldsymbol{\nabla} q = -\frac{\rho}{\tau} \int_\Omega (\boldsymbol{u}_m^{n+1} - \boldsymbol{u}_m^n) \cdot \boldsymbol{\nabla} q - \rho \int_\Omega (\boldsymbol{u}_m^{n+1/2} \cdot \boldsymbol{\nabla} \boldsymbol{u}_m^{n+1/2}) \cdot \boldsymbol{\nabla} q \tag{3}$$

for all $q \in \mathcal{P}_{1,h}$, and $p_{\text{ppe}} = q = 0$ on Γ_o.

Note that we leave out the term $\Delta \boldsymbol{u}_m^{n+1/2}$ since it was reported in [8] that the viscous part of the pressure gradient in large vessels is negligible. Moreover, since $\boldsymbol{u}_m^n \in \mathcal{P}_{1,h}$, the data does not possess enough regularity to compute its laplacian.

Then, the pressure drop at time $t^{n+1/2}$ between the outlet and the inlet is evaluated with Equation (2) using $p = p_{\text{ppe}}^{n+1/2}$. Note also that the midpoint time evaluation scheme allows a second order approximation with respect to time and to reduce the noise variance of the measurements $\boldsymbol{u}_m^{n+1/2}$ by a factor of 2 with respect to the original variance of the measurements $\boldsymbol{u}_m^n$.

3.2 The Stokes estimator (STE)

The STE formulated in [10] consists in perturbing the Navier–Stokes equation with the Laplacian of an auxiliary divergence-free velocity field $\boldsymbol{w}$. This leads to a mixed problem for the pressure, in terms of the measured velocity, instead of a Poisson problem as in the PPE.

Defining $\mathcal{P}_{1,h}^b$ as the finite element space with linear piecewise polynomials with an additional bubble function at the centroid of the element, the STE is formulated as follows for

the time step $t^{n+1/2}$: Find $\boldsymbol{w} \in [\mathcal{P}^b_{1,h}]^d$ and $p^{n+1/2}_{ste} \in \mathcal{P}_{1,h}$, such that

$$\begin{aligned}\int_\Omega \boldsymbol{\nabla w} : \boldsymbol{\nabla \hat{w}} - \int_\Omega p^{n+1/2}_{ste}(\boldsymbol{\nabla}\cdot\hat{\boldsymbol{w}}) + \int_\Omega (\boldsymbol{\nabla}\cdot\boldsymbol{w})q &= -\frac{\rho}{\tau}\int_\Omega (\boldsymbol{u}^{n+1}_m - \boldsymbol{u}^n_m)\cdot\hat{\boldsymbol{w}} \\ &\quad -\rho\int_\Omega (\boldsymbol{u}^{n+1/2}_m \cdot \boldsymbol{\nabla u}^{n+1/2}_m)\cdot\hat{\boldsymbol{w}} \quad (4)\end{aligned}$$

for all $\hat{\boldsymbol{w}} \in [\mathcal{P}^b_{1,h}]^d$ and $q \in \mathcal{P}_{1,h}$, with $\boldsymbol{w} = \hat{\boldsymbol{w}} = \boldsymbol{0}$ on Γ. Then, the pressure drop at time $t^{n+1/2}$ between the outlet and the inlet is evaluated with Formula (2) using $p = p^{n+1/2}_{\text{ste}}$. We remark that no additional information on the pressure field $p^{n+1/2}_{ste}$ is needed for ensuring solvability of Problem (4). Notice also that, as for the PPE, the viscous term is neglected.

3.3 The work-energy relative pressure estimator (WERP)

The starting point of the formulation of the WERP method introduced in [3] is the classical energy relation of an incompressible Newtonian fluid, which can be obtained either by writing the conservation law for the energy density $\rho\boldsymbol{u}^2/2$ directly or multiplying (1) by $\boldsymbol{u}$ and integrating over Ω. This relation reads

$$\frac{\rho}{2}\int_\Omega \partial_t(|\boldsymbol{u}|^2) + \frac{\rho}{2}\int_\Gamma (\boldsymbol{u}\cdot\boldsymbol{n})|\boldsymbol{u}|^2 + \mu\int_\Omega |\boldsymbol{\nabla u}|^2 + \int_\Gamma p\,(\boldsymbol{u}\cdot\boldsymbol{n}) - \mu\int_\Gamma (\boldsymbol{\nabla u}\cdot\boldsymbol{n})\cdot\boldsymbol{u} = 0\ , \quad (5)$$

with $|\cdot|$ denoting the Euclidian norm.

The WERP is then formulated by assuming that: (i) the measurements $\boldsymbol{u}^n_m$ satisfy relation (5), (ii) $\boldsymbol{u}^n_m \cdot \boldsymbol{n} \approx 0$ on Γ_w (i.e. the vessel walls nearly don't move), (iii) the viscous forces on Γ are negligible, (iv) and the pressure is nearly constant on Γ_i and Γ_o. Doing so, the WERP pressure estimator at time $t^{n+1/2}$ is written as:

$$\delta p^{n+1/2}_{werp}(\boldsymbol{u}^{n,n+1}_m) = \frac{-1}{\Lambda(\boldsymbol{u}^{n+1/2}_m)}\left(E_{kin}(\boldsymbol{u}^{n+1}_m) - E_{kin}(\boldsymbol{u}^n_m) + E_{conv}(\boldsymbol{u}^{n+1/2}_m) + E_{visc}(\boldsymbol{u}^{n+1/2}_m)\right) \quad (6)$$

with

$$E_{kin}(\boldsymbol{w}) = \frac{\rho}{2\tau}\int_\Omega |\boldsymbol{w}|^2 \quad (7)$$

$$E_{conv}(\boldsymbol{w}) = \frac{\rho}{2}\int_{\Gamma_i\cup\Gamma_o} (\boldsymbol{w}\cdot\boldsymbol{n})|\boldsymbol{w}|^2 \quad (8)$$

$$E_{visc}(\boldsymbol{w}) = \mu\int_\Omega |\boldsymbol{\nabla w}|^2 \quad (9)$$

$$\Lambda(\boldsymbol{w}) = \int_{\Gamma_i} \boldsymbol{w}\cdot\boldsymbol{n}. \quad (10)$$

Note that the superscript $n, n+1$ means that both velocity at the measured time steps n and $n+1$ are considered.

As it is well known from numerical analysis, the use of the mid-point scheme in (6) does not induce any perturbation compared with the time-continuous energy relation (5), independently on the time step τ.

We can see that this formulation may be unstable at small in-/outflows due to the division by $\Lambda(\boldsymbol{u}_m^{n+1/2})$. In other words, when the inflow is small, perturbations (e.g. due to the presence of measurement noise) can induce large errors in $\Lambda(\boldsymbol{u}_m^{n+1/2})$ leading to an unphysical amplification of the estimated relative pressure. Fortunately, low flow regimes are not relevant in clinical practice since only peak relative pressures are of interest. Another important issue is that the WERP induces systematic shifts in the pressure curve in the presence of noise, as we will see in the next section. Moreover, the WERP can only by construction estimate relative pressure in geometries with only one inflow and one outflow, due to the assumption $\boldsymbol{u}_m^n \cdot \boldsymbol{n} \approx 0$ on Γ_w needed to eliminate the pressure field on Γ_w out of the formulation.

4 New estimation methods

In this section we present new pressure estimation methods, inspired from the state-of-the-art approaches, and we will see later in the numerical examples that they can lead to improvements in the estimation results.

4.1 The integrated STE (STEint)

We propose to modify the STE method originally proposed in [10] and formulated in Equation (4) by taking advantage of the regularity of the auxiliary velocity field and integrating the convective and viscous terms by parts.

The STEint is formulated as follows for the time step $t^{n+1/2}$. Find $\boldsymbol{w} \in [\mathcal{P}_{1,h}^b]^d$ and $p_{stei}^{n+1/2} \in \mathcal{P}_{1,h}$, such that

$$\begin{aligned}\int_\Omega \boldsymbol{\nabla w} : \boldsymbol{\nabla \hat{w}} - \int_\Omega p_{stei}^{n+1/2}(\boldsymbol{\nabla}\cdot\hat{\boldsymbol{w}}) + \int_\Omega (\boldsymbol{\nabla}\cdot\boldsymbol{w})q \;\; = \;\; & -\frac{\rho}{\tau}\int_\Omega (\boldsymbol{u}_m^{n+1}-\boldsymbol{u}_m^n)\cdot\hat{\boldsymbol{w}} \\ & +\rho\int_\Omega (\boldsymbol{u}_m^{n+1/2}\cdot\boldsymbol{\nabla}\hat{\boldsymbol{w}})\cdot\boldsymbol{u}_m^{n+1/2} \\ & -\mu\int_\Omega \boldsymbol{\nabla u}_m^{n+1/2} : \boldsymbol{\nabla}\hat{\boldsymbol{w}} \qquad (11)\end{aligned}$$

for all $\hat{\boldsymbol{w}} \in [\mathcal{P}_{1,h}^b]^d$ and $q \in \mathcal{P}_{1,h}$, with $\boldsymbol{w} = \hat{\boldsymbol{w}} = \boldsymbol{0}$ on Γ. Notice that the boundary terms of the integration by parts do not appear since $\hat{\boldsymbol{w}} = \boldsymbol{0}$. Then, the pressure drop at time $t^{n+1/2}$ between the outlet and the inlet is evaluated with Formula (2) using $p = p_{\text{stei}}^{n+1/2}$.

The advantage of reducing the derivative order of the measurements will be noticeable in the robustness of the pressure estimation results when spatially subsampling the data. Unfortunately, this integration by parts is not straightforward for the PPE method due to the lack of enough regularity of $\boldsymbol{\nabla} q$ in Equation (3) when standard piecewise polynomial finite element spaces are used (like $\mathcal{P}_{1,h}$).

4.2 The Darcy estimator (DAE)

Note that, a similar alternative for the STE would be to use a Darcy formulation for $\boldsymbol{w}$ instead of Stokes. Let $\mathcal{RT}_h^k$ be the usual Raviart-Thomas finite element space of degree k. Then, find $\boldsymbol{w} \in \mathcal{RT}_h^1$ and $p_{\text{dae}}^{n+1/2} \in \mathcal{P}_{1,h}$, such that

$$\begin{aligned}\int_\Omega \boldsymbol{w}\cdot\hat{\boldsymbol{w}} - \int_\Omega p_{\text{dae}}^{n+1/2}(\boldsymbol{\nabla}\cdot\hat{\boldsymbol{w}}) + \int_\Omega (\boldsymbol{\nabla}\cdot\boldsymbol{w})q &= -\frac{\rho}{\tau}\int_\Omega (\boldsymbol{u}_m^{n+1}-\boldsymbol{u}_m^n)\cdot\hat{\boldsymbol{w}} \\ &\quad -\rho\int_\Omega (\boldsymbol{u}_m^{n+1/2}\cdot\boldsymbol{\nabla}\boldsymbol{u}_m^{n+1/2})\cdot\hat{\boldsymbol{w}} \end{aligned} \tag{12}$$

for all $\hat{\boldsymbol{w}} \in \mathcal{RT}_h^1$ and $q \in \mathcal{P}_{1,h}$, with $\boldsymbol{w}\cdot\boldsymbol{n} = \hat{\boldsymbol{w}}\cdot\boldsymbol{n} = 0$ on Γ. This approach has not yet been reported, to the best of the authors knowledge. Note also that here the integration by parts of the convective and viscous terms of the right-hand side, as by the STEint, is for formal reasons not possible since $\hat{\boldsymbol{w}} \in \mathcal{H}_{\text{div}}(\Omega)$ and it can be easily shown that $\mathcal{H}_1(\Omega) \subset \mathcal{H}_{\text{div}}(\Omega)$.

4.3 Integral momentum relative pressure estimator (IMRP)

In this section we derive a new formulation for the integral relative pressure estimator based on a general class of test functions.

Assume that we have computed some specific function $\boldsymbol{v} \in \mathcal{H}_1(\Omega)$ satisfying

$$\boldsymbol{\nabla}\cdot\boldsymbol{v} \approx 0 \ , \ \boldsymbol{v}\cdot\boldsymbol{n} = 0 \text{ on } \Gamma_w \tag{13}$$

If we multiply Equation $(1)_1$ by $\boldsymbol{v}$ and we integrate over Ω

$$\underbrace{\rho\int_\Omega \partial_t\boldsymbol{u}\cdot\boldsymbol{v}}_{I_{kin}(\partial_t\boldsymbol{u})} + \underbrace{\rho\int_\Omega (\boldsymbol{u}\cdot\boldsymbol{\nabla}\boldsymbol{u})\cdot\boldsymbol{v}}_{I_{conv}(\boldsymbol{u})} + \underbrace{\int_\Omega \boldsymbol{\nabla}p\cdot\boldsymbol{v}}_{I_{pres}} \underbrace{-\mu\int_\Omega \Delta\boldsymbol{u}\cdot\boldsymbol{v}}_{I_{visc}(\boldsymbol{u})} = 0 \ . \tag{14}$$

we obtain for each of the terms

$$I_{conv}(\boldsymbol{u}) = -\rho\int_\Omega (\boldsymbol{u}\cdot\boldsymbol{\nabla}\boldsymbol{v})\cdot\boldsymbol{u} + \rho\int_\Gamma (\boldsymbol{u}\cdot\boldsymbol{n})(\boldsymbol{u}\cdot\boldsymbol{v}) \tag{15}$$

$$I_{pres} = -\int_\Omega p(\boldsymbol{\nabla}\cdot\boldsymbol{v}) + \int_\Gamma p\,(\boldsymbol{v}\cdot\boldsymbol{n}) = \int_{\Gamma_i\cup\Gamma_o} p\,(\boldsymbol{v}\cdot\boldsymbol{n}) \tag{16}$$

$$I_{visc}(\boldsymbol{u}) = \mu\int_\Omega \boldsymbol{\nabla}\boldsymbol{u} : \boldsymbol{\nabla}\boldsymbol{v} - \mu\int_\Gamma (\boldsymbol{\nabla}\boldsymbol{u}\cdot\boldsymbol{n})\cdot\boldsymbol{v} \tag{17}$$

using standard integration by parts.

The integral momentum relative pressure estimator (IMRP) is then formulated by assuming that: (i) the measurements $\boldsymbol{u}_m^n$ satisfy relation (14), (ii) the pressure is nearly constant on Γ_i and Γ_o. Doing so, the IMRP estimator at time $t^{n+1/2}$ is formulated as:

$$\delta p_{\text{imrp}}^{n+1/2}(\boldsymbol{u}_m^{n,n+1}) = -\frac{1}{\Lambda(\boldsymbol{v})}\left(I_{kin}(\frac{\boldsymbol{u}_m^{n+1}-\boldsymbol{u}_m^n}{\tau}) + I_{conv}(\boldsymbol{u}_m^{n+1/2}) + I_{visc}(\boldsymbol{u}_m^{n+1/2})\right) \ . \tag{18}$$

Note that the requirements on the function in (13) serve only so that the pressure field vanishes (up to the relative pressure) in (16).

Notice also that the integral terms $I_{kin}, I_{conv}, I_{visc}$ are multiplied by $1/\Lambda(\boldsymbol{v})$ in the estimator formulation, which is independent of the measurements. This is an advantage compared to the WERP for the potential spurious amplifications for low flows. Another advantage will be clear after the bias analysis. We also point out that we did not make any assumption on the velocity measurements on the boundary Γ_w, as it was done for the WERP. Hence it is potentially better at capturing the pressure gradient changes due to the wall deformation.

We propose the test function $\boldsymbol{v}$ as the solution of the following Poiseuille flow, i.e. a Stokes flow solution with unitary Neumann load on Γ_i: Find $\boldsymbol{v} \in [\mathcal{P}^b_{1,h}]^d$ and $z \in \mathcal{P}_{1,h}$,

$$\int_\Omega \boldsymbol{\nabla v} : \boldsymbol{\nabla \psi} + \int_\Omega z \boldsymbol{\nabla} \cdot \boldsymbol{\psi} + \int_\Omega q \boldsymbol{\nabla} \cdot \boldsymbol{v} + \int_{\Gamma_i} \boldsymbol{\psi} \cdot \boldsymbol{n} = 0 \ , \tag{19}$$

for all $\boldsymbol{\psi} \in [\mathcal{P}^b_{1,h}]^d$ and $q \in \mathcal{P}_{1,h}$, and with $\boldsymbol{v} = \boldsymbol{\psi} = \boldsymbol{0}$ on Γ_w. It is not necessary to introduce any coefficient in the viscous term in (19) since the IMRP estimator is independent of any constant scaling of the velocity field, see Equation (18). The same applies to the unitary Neumann load in (19). Note also that in the specific choice of this auxiliary function, since $\boldsymbol{v} = \boldsymbol{\psi} = \boldsymbol{0}$ on Γ_w all terms in that boundary in (15)-(17) vanish.

Remark 1. *The final relative pressure estimation seems to not considerably depend on the order of the finite element space used for the test function in the numerical experiments. Differences between the different spaces can only be appreciated for coarse mesh spacing of the measurements, i.e. larger than* 3 *mm. The same applies to the discretization of the STE, STEint and DAE mixed problems.*

5 Bias analysis

We remind the reader that we deal with additive random perturbations of the measured (subsampled) velocity. In this section we detail then how to compute the bias of the estimation methods introduced previously, what has not been done in all original works (i.e for PPE, STE and WERP), to the best of the authors knowledge.

5.1 Generalities

The computation of the bias implies in practice to calculate the following quantity:

$$\mathbb{E}\left(\delta p^{n+1/2}(\boldsymbol{u}_h^{n,n+1} + \boldsymbol{\varepsilon}^{n,n+1})\right) - \delta p^{n+1/2}(\boldsymbol{u}_h^{n,n+1}) \tag{20}$$

with $\mathbb{E}$ the usual expected value operator. Notice that it does not take into account the estimation errors due to the spatial or temporal subsampling. In simple words, bias is how much the mean of the estimators when including noise in the measurements differ from the estimator with noise-free measurements.

Since $\boldsymbol{\varepsilon}^n \in [\mathcal{P}_{1,h}]^d$ is a discrete noise field we can write it (using the Einstein summation convention from now on) as $\boldsymbol{\varepsilon}_i^n(\boldsymbol{x}) = N_j(\boldsymbol{x}) e_{i,j}^n$, with $N_j(\boldsymbol{x})$ the finite element shape function for the j-th degree-of-freedom of $\mathcal{P}_{1,h}$ and i denotes the spatial direction.

Remember also that the degrees-of-freedom $e_{i,j}^n$ are independently identically distributed (i.i.d.) following a normal distribution $\mathcal{N}(0, \sigma^2)$ for all n, i, j. For any linear, differential operator with deterministic coefficients $\mathbb{D} : \mathcal{H}_1(\Omega) \to \mathcal{L}_2(\Omega)$ we have therefore the following Identity:

$$\mathbb{E}\left(\int_\Omega \mathbb{D}(\boldsymbol{\varepsilon}_i^n)\right) = \int_\Omega \mathbb{E}\left(e_{i,j}^n\right) \mathbb{D}(N_j(\boldsymbol{x})) = 0 \tag{21}$$

5.2 PPE

To compute then the bias (20) for the PPE method we proceed as follows. Note that the bias function $b_{\text{ppe}} := \mathbb{E}(p_{\text{ppe}}^{n+1/2}(\boldsymbol{u}_m^{n,n+1})) - p_{\text{ppe}}^{n+1/2}(\boldsymbol{u}_h^{n,n+1})$ satisfies the problem: Find $b_{\text{ppe}} \in \mathcal{P}_{1,h}$ such that

$$\begin{aligned}\int_\Omega \boldsymbol{\nabla} b_{\text{ppe}} \cdot \boldsymbol{\nabla} q \;\; = \;\; & \mathbb{E}\left(-\frac{\rho}{\tau}\int_\Omega (\boldsymbol{u}_m^{n+1} - \boldsymbol{u}_m^n)\cdot\boldsymbol{\nabla} q\right) + \frac{\rho}{\tau}\int_\Omega (\boldsymbol{u}_h^{n+1} - \boldsymbol{u}_h^n)\cdot\boldsymbol{\nabla} q \\ & -\mathbb{E}\left(\rho\int_\Omega (\boldsymbol{u}_m^{n+1/2}\cdot\boldsymbol{\nabla}\boldsymbol{u}_m^{n+1/2})\cdot\boldsymbol{\nabla} q\right) + \rho\int_\Omega (\boldsymbol{u}_h^{n+1/2}\cdot\boldsymbol{\nabla}\boldsymbol{u}_h^{n+1/2})\cdot\boldsymbol{\nabla} q\end{aligned} \tag{22}$$

for all $q \in \mathcal{P}_{1,h}$, and $b_{\text{ppe}} = q = 0$ on Γ_o. Since $\boldsymbol{u}_m^n = \boldsymbol{u}_h^n + \boldsymbol{\varepsilon}^n$, the kinetic terms of the right-hand-side of Problem (22) are zero due to Identity (21). For the convective terms, the only ones surviving are (since the expected value of the cross terms is zero due to Identity (21))

$$\begin{aligned}\rho\int_\Omega \mathbb{E}\left((\boldsymbol{\varepsilon}^{n+1/2}\cdot\boldsymbol{\nabla}\boldsymbol{\varepsilon}^{n+1/2})\right)\cdot\boldsymbol{\nabla} q \;\; &= \;\; \rho\int_\Omega \mathbb{E}\left(\boldsymbol{\varepsilon}_k^{n+1/2}\partial_k\boldsymbol{\varepsilon}_i^{n+1/2}\right)\partial_i q \\ &= \;\; \rho\int_\Omega \mathbb{E}\left(N_j e_{k,j}^{n+1/2}\partial_k(N_\ell e_{i,\ell}^{n+1/2})\right)\partial_i q \\ &= \;\; \rho\int_\Omega \mathbb{E}\left(e_{k,j}^{n+1/2}e_{i,\ell}^{n+1/2}\right) N_j\partial_k N_\ell\partial_i q \\ &= \;\; \rho\int_\Omega \frac{\sigma^2}{2} N_j\partial_k N_j\partial_k q = \frac{\rho\sigma^2}{4}\int_\Omega \partial_k\sum_j (N_j)^2\partial_k q \\ &= \;\; \frac{\rho\sigma^2}{4}\int_\Omega \boldsymbol{\nabla}\alpha\cdot\boldsymbol{\nabla} q\end{aligned}$$

with $\alpha = \sum_j (N_j)^2$ in $\mathcal{P}_{2,h}$. Therefore, we can compute the bias spatial distribution b_{ppe} by solving:

$$\int_\Omega \boldsymbol{\nabla} b_{\text{ppe}}\cdot\boldsymbol{\nabla} q = -\frac{\rho\sigma^2}{4}\int_\Omega \boldsymbol{\nabla}\alpha\cdot\boldsymbol{\nabla} q\ . \tag{23}$$

with $b_{\text{ppe}} = q = 0$ on Γ_o. Finally, the bias for the relative pressure δp can be computed by evaluating Formula (2) with $p = b_{\text{ppe}}$.

We want to remark that this expression provides a closed form for the bias, depending on known constants and the geometry itself, and it is independent of the real velocity field and hence also of time. Therefore, it can be always evaluated a priori and in the numerical examples we will verify that it is absolutely negligible with respect to the relative pressure of interest. This will be also the case with the rest of the methods, except WERP.

5.3 STE and DAE

Analogous to the PPE case, since they all share the same form for the right-hand-side, the bias of STE and DAE can be computed by solving the following problems.

For the STE: Find $\boldsymbol{w} \in [\mathcal{P}^b_{1,h}]^d$ and $b_{\text{ste}} \in \mathcal{P}_{1,h}$, such that

$$\int_\Omega \boldsymbol{\nabla w} : \boldsymbol{\nabla \hat{w}} - \int_\Omega b_{\text{ste}}(\boldsymbol{\nabla} \cdot \hat{\boldsymbol{w}}) + \int_\Omega (\boldsymbol{\nabla} \cdot \boldsymbol{w}) q \;=\; -\frac{\rho\sigma^2}{4} \int_\Omega \boldsymbol{\nabla}\alpha \cdot \hat{\boldsymbol{w}} \tag{24}$$

for all $\hat{\boldsymbol{w}} \in [\mathcal{P}^b_{1,h}]^d$ and $q \in \mathcal{P}_{1,h}$, with $\boldsymbol{w} = \hat{\boldsymbol{w}} = \boldsymbol{0}$ on Γ.

And now for the DAE: Find $\boldsymbol{w} \in \mathcal{RT}^1_h$ and $b_{\text{dae}} \in \mathcal{P}_{1,h}$, such that

$$\int_\Omega \boldsymbol{w} \cdot \hat{\boldsymbol{w}} - \int_\Omega b_{\text{dae}}(\boldsymbol{\nabla} \cdot \hat{\boldsymbol{w}}) + \int_\Omega (\boldsymbol{\nabla} \cdot \boldsymbol{w}) q \;=\; -\frac{\rho\sigma^2}{4} \int_\Omega \boldsymbol{\nabla}\alpha \cdot \hat{\boldsymbol{w}} \tag{25}$$

for all $\hat{\boldsymbol{w}} \in \mathcal{RT}^1_h$ and $q \in \mathcal{P}_{1,h}$, with $\boldsymbol{w} \cdot \boldsymbol{n} = \hat{\boldsymbol{w}} \cdot \boldsymbol{n} = 0$ on Γ.

5.4 STEint

Due to the integration by parts in the right-hand-side, the STEint case has to be handled slightly different. Again, due to Identity (21) the kinetic, and now also the viscous terms in the right-hand-side of the bias equation, vanish. The only surviving term in the convective part has the form:

$$\begin{aligned} \rho \int_\Omega \mathbb{E}\left((\boldsymbol{\varepsilon}^{n+1/2} \cdot \boldsymbol{\nabla}\hat{\boldsymbol{w}}) \cdot \boldsymbol{\varepsilon}^{n+1/2}\right) &= \rho \int_\Omega \mathbb{E}\left(\boldsymbol{\varepsilon}_i^{n+1/2} \partial_i \hat{\boldsymbol{w}}_j \boldsymbol{\varepsilon}_j^{n+1/2}\right) \\ &= \rho \int_\Omega \mathbb{E}\left(e_{i,k}^{n+1/2} e_{j,\ell}^{n+1/2}\right) N_k N_\ell \partial_i \hat{\boldsymbol{w}}_j = \frac{\rho\sigma^2}{2} \int_\Omega \alpha \boldsymbol{\nabla} \cdot \hat{\boldsymbol{w}} \end{aligned} \tag{26}$$

Therefore, for the STEint the bias equation reads: Find $\boldsymbol{w} \in [\mathcal{P}^b_{1,h}]^d$ and $b_{\text{stei}} \in \mathcal{P}_{1,h}$, such that

$$\int_\Omega \boldsymbol{\nabla w} : \boldsymbol{\nabla \hat{w}} - \int_\Omega b_{\text{stei}}(\boldsymbol{\nabla} \cdot \hat{\boldsymbol{w}}) + \int_\Omega (\boldsymbol{\nabla} \cdot \boldsymbol{w}) q \;=\; \frac{\rho\sigma^2}{2} \int_\Omega \alpha \boldsymbol{\nabla} \cdot \hat{\boldsymbol{w}} \tag{27}$$

for all $\hat{\boldsymbol{w}} \in [\mathcal{P}^b_{1,h}]^d$ and $q \in \mathcal{P}_{1,h}$, with $\boldsymbol{w} = \hat{\boldsymbol{w}} = \boldsymbol{0}$ on Γ.

5.5 IMRP

The bias of the IMRP can be directly defined as

$$b_{\text{irmp}} = \mathbb{E}(\delta p_{\text{imrp}}^{n+1/2}(\boldsymbol{u}_m^{n,n+1})) - \delta p_{\text{imrp}}^{n+1/2}(\boldsymbol{u}_h^{n,n+1})$$

It can be easily verified that due to Identity (21) the bias expression reduces to convective terms only:

$$\begin{aligned} b_{\text{irmp}} &= -\frac{1}{\Lambda(\boldsymbol{v})}\left(-\rho\int_\Omega \mathbb{E}\left(\boldsymbol{\varepsilon}_i^{n+1/2}\partial_j \boldsymbol{v}_i \boldsymbol{\varepsilon}_j^{n+1/2}\right) + \rho\int_\Gamma \mathbb{E}(\boldsymbol{\varepsilon}_i^{n+1/2}\boldsymbol{n}_i\boldsymbol{\varepsilon}_j^{n+1/2}\boldsymbol{v}_j)\right) \\ &= \frac{\rho\sigma^2}{2\Lambda(\boldsymbol{v})}\int_\Omega \alpha\boldsymbol{\nabla}\cdot\boldsymbol{v} - \frac{\rho}{\Lambda(\boldsymbol{v})}\int_\Gamma N_k N_\ell \boldsymbol{n}_i\boldsymbol{v}_j\mathbb{E}(e_{i,k}^{n+1/2}e_{j,\ell}^{n+1/2}) \\ &= \frac{\rho\sigma^2}{2\Lambda(\boldsymbol{v})}\int_\Omega \alpha\boldsymbol{\nabla}\cdot\boldsymbol{v} - \frac{\rho\sigma^2}{2\Lambda(\boldsymbol{v})}\int_\Gamma \alpha\boldsymbol{v}\cdot\boldsymbol{n}\ . \end{aligned}$$

5.6 WERP

We will now end the bias analysis with the WERP estimator. We will need for the analysis the following additional identities:

$$\mathbb{E}\left(\rho\int_\Omega |\boldsymbol{\varepsilon}^n|^2\right) = \sigma^2\,\mathrm{tr}(\boldsymbol{M}_\Omega),\ \mathbb{E}\left(\mu\int_\Omega |\boldsymbol{\nabla}\boldsymbol{\varepsilon}^{n+1/2}|^2\right) = \frac{\sigma^2}{2}\,\mathrm{tr}(\boldsymbol{K}_\Omega)\ , \tag{28}$$

with $\boldsymbol{M}_\Omega$ and $\boldsymbol{K}_\Omega$ the classical mass and stiffness finite element matrices for the Stokes problem in $\mathcal{P}_{1,h}$, respectively. Then, let us point out that the following identities hold:

The goal is now to compute:

$$b_{\text{werp}} = \mathbb{E}(\delta p_{\text{werp}}^{n+1/2}(\boldsymbol{u}_m^{n,n+1})) - \delta p_{\text{werp}}^{n+1/2}(\boldsymbol{u}_h^{n,n+1})$$

In order to perform such an analysis, we include an additional assumption that $\Lambda(\boldsymbol{u}_m^{n+1/2}) \approx \Lambda(\boldsymbol{u}_h^{n+1/2})$, what is reasonable if we are interested in estimating the peak systolic relative pressure, which typically is simultaneous to the peak flow where the signal-to-noise ratio is best.

We proceed therefore as follows:

$$\mathbb{E}(\delta p_{werp}^{n+1/2}(\boldsymbol{u}_m^{n,n+1})) \approx \frac{-1}{\Lambda(\boldsymbol{u}_m^{n+1/2})}\mathbb{E}\left(E_{kin}(\boldsymbol{u}_m^{n+1}) - E_{kin}(\boldsymbol{u}_m^n) + E_{conv}(\boldsymbol{u}_m^{n+1/2}) + E_{visc}(\boldsymbol{u}_m^{n+1/2})\right)\ . \tag{29}$$

We now compute separately each term. First the kinetic part

$$\begin{aligned} \mathbb{E}\left(E_{kin}(\boldsymbol{u}_m^n)\right) &= \mathbb{E}\left(\frac{\rho}{2\tau}\int_\Omega |\boldsymbol{u}_h^n + \boldsymbol{\varepsilon}^n|^2\right) \\ &= \frac{\rho}{2\tau}\int_\Omega \mathbb{E}\left(|\boldsymbol{u}_h^n|^2 + 2\boldsymbol{u}_h^n\cdot\boldsymbol{\varepsilon}^n + |\boldsymbol{\varepsilon}^n|^2\right) \\ &= E_{kin}(\boldsymbol{u}_h^n) + \frac{\sigma^2}{2\tau}\,\mathrm{tr}(\boldsymbol{M}_\Omega)\ . \end{aligned}$$

Then, the convective part can be reduced using Identity (21):

$$\begin{aligned}
\mathbb{E}\left(E_{conv}(\boldsymbol{u}_m^n)\right) &= \frac{\rho}{2}\int_{\Gamma_i\cup\Gamma_o}\mathbb{E}\left(((\boldsymbol{u}_h^n+\boldsymbol{\varepsilon}^n)\cdot\boldsymbol{n})|\boldsymbol{u}_h^n+\boldsymbol{\varepsilon}^n|^2\right)\\
&= \frac{\rho}{2}\int_{\Gamma_i\cup\Gamma_o}\mathbb{E}\big((\boldsymbol{u}_h^n\cdot\boldsymbol{n})\left\{|\boldsymbol{u}_h^n|^2+2\boldsymbol{u}_h^n\cdot\boldsymbol{\varepsilon}^n+|\boldsymbol{\varepsilon}^n|^2\right\}\\
&\qquad +(\boldsymbol{\varepsilon}^n\cdot\boldsymbol{n})\left\{|\boldsymbol{u}_h^n|^2+2\boldsymbol{u}_h^n\cdot\boldsymbol{\varepsilon}^n+|\boldsymbol{\varepsilon}^n|^2\right\}\big)\\
&= E_{conv}(\boldsymbol{u}_h^n)+\frac{\rho}{2}\int_{\Gamma_i\cup\Gamma_o}\mathbb{E}\left((\boldsymbol{u}_h^n\cdot\boldsymbol{n})|\boldsymbol{\varepsilon}^n|^2+2(\boldsymbol{\varepsilon}^n\cdot\boldsymbol{n})(\boldsymbol{u}_h^n\cdot\boldsymbol{\varepsilon}^n)\right)
\end{aligned}$$

where it can be easily shown that the very last (cubic) term in the second row vanishes due to the standard result that the cube of a normal variable has also zero expected value. Now we continue using the fact that $\boldsymbol{\varepsilon}_i^n = N_j e_{i,j}^n$

$$\begin{aligned}
\mathbb{E}\left(E_{conv}(\boldsymbol{u}_m^n)\right) &= E_{conv}(\boldsymbol{u}_h^n)+\frac{\rho}{2}\int_{\Gamma_i\cup\Gamma_o}(\boldsymbol{u}_h^n\cdot\boldsymbol{n})\sum_i\mathbb{E}\left((N_j e_{i,j}^n)^2\right)+2\mathbb{E}\left((\boldsymbol{\varepsilon}^n\cdot\boldsymbol{n})(\boldsymbol{u}_h^n\cdot\boldsymbol{\varepsilon}^n)\right)\\
&= E_{conv}(\boldsymbol{u}_h^n)+\frac{\rho}{2}\int_{\Gamma_i\cup\Gamma_o}(\boldsymbol{u}_h^n\cdot\boldsymbol{n})(d\sigma^2)\alpha+2\mathbb{E}\left((N_k e_{i,k}^n)(N_\ell e_{j,\ell}^n)\right)\boldsymbol{n}_i\boldsymbol{u}_{h,j}^n\\
&= E_{conv}(\boldsymbol{u}_h^n)+\frac{\rho}{2}\int_{\Gamma_i\cup\Gamma_o}(\boldsymbol{u}_h^n\cdot\boldsymbol{n})(d\sigma^2)\alpha+2\sigma^2\alpha\boldsymbol{u}_h^n\cdot\boldsymbol{n}\\
&= E_{conv}(\boldsymbol{u}_h^n)+B_{conv}(\boldsymbol{u}_h^n,\sigma^2)\ ,\ B_{conv}(\boldsymbol{u}_h^n,\sigma^2)=\frac{\rho\sigma^2(d+2)}{2}\int_{\Gamma_i\cup\Gamma_o}(\boldsymbol{u}_h^n\cdot\boldsymbol{n})\alpha
\end{aligned}$$

with d the spatial dimension (in our examples later $d=3$). And at last, the viscous part

$$\begin{aligned}
\mathbb{E}\left(E_{visc}(\boldsymbol{u}_m^{n+1/2})\right) &= E_{visc}(\boldsymbol{u}_h^{n+1/2})+\mu\int_\Omega 2\boldsymbol{\nabla}\boldsymbol{u}_h^{n+1/2}:\boldsymbol{\nabla}\boldsymbol{\varepsilon}^{n+1/2}+|\boldsymbol{\nabla}\boldsymbol{\varepsilon}^{n+1/2}|^2\\
&= E_{visc}(\boldsymbol{u}_h^{n+1/2})+\frac{\sigma^2}{2}\operatorname{tr}(\boldsymbol{K}_\Omega)\ .
\end{aligned}$$

Now, we inserted the computed expected values into Equation (29) and we then obtain the following expression for the bias of the WERP estimator

$$b_{\text{werp}}\approx\frac{-1}{\Lambda(\boldsymbol{u}_m^{n+1/2})}\left(\frac{1}{2}B_{conv}(\boldsymbol{u}_h^{n+1/2},\sigma^2)+\frac{\sigma^2}{2}\operatorname{tr}(\boldsymbol{K}_\Omega)\right)\ . \tag{30}$$

Note that B_{conv} depends on both real (unknown) spatially subsampled velocity $\boldsymbol{u}_h^{n+1/2}$ and noise variance σ^2, while the second term of the bias depends on σ^2 and the geometry Ω only. However, we will show in the examples that this term is very small B_{conv} compared with the viscous part of the bias.

Remark 2. *It is not straightforward to perform similar computations for the variance of the estimators. For the PPE, STE, STEint and DAE, no expression or equation (to our knowledge) can be formulated. For the WERP and IMRP, even though the expressions for the pressure drop are explicit, in the variance the expected value of products of integrals containing the noise is needed. This can not be computed as before since these integrals are not i.i.d.*

6 Numerical examples

6.1 Forward simulations

The synthetic measurements are obtained from a Navier-Stokes simulation in a three-dimensional geometry representing a stenotic blood vessel, see Figure 1. The radii of inlet and outlet are 1 cm and the stenosis has a radius of 0.4 cm, i.e. 60 % of coarctation. The physical parameters were chosen as $\mu = 0.035$ Poise and $\rho = 1.0$ gr/cm^3. An homogeneous Neumann load on Γ_o was imposed, while an homogeneous Dirichlet condition on Γ_w and the following Dirichlet condition on Γ_i are considered:

$$\boldsymbol{u} = 60(x^2 + z^2 - 1)\sin\left(\frac{5\pi}{2}t\right)\boldsymbol{n} \quad \text{on } \Gamma_w \tag{31}$$

where x, z are the coordinates of the plane perpendicular to the main flow direction (the vessel centerline lies on $x = z = 0$). This input data leads to a peak inflow rate and pressure drop of 94 cm^3/s and 21 mmHg, respectively. This pressure drop is typical from transitional coarctations from mild to severe and represents a typical threshold for clinical decisions [13].

The numerical solution of the reference problem was performed using a monolithic velocity-pressure coupling. The space-semi-discretization was performed with $\mathcal{P}^b_{1,h}/\mathcal{P}_{1,h}$ finite elements for the velocity and pressure, respectively, with a mesh spacing of $h = 0.06$ cm. A backward Euler scheme was used for the time-semi-discretization with time-step of 0.002 s, with a semi-implicit treatment of the convective term, and including a Temam stabilization term to ensure Lyapunov stability of the solution in time [11]. At that spatial refinement level, no volume or backflow convective instabilities were observed, so no volume convective or backflow stabilization terms were included in order to not perturb the original equation, e.g. SUPG [2] or backflow stabilization [1].

6.2 Synthetic measurements

Synthetic measurements (see Figure 2) were generated considering the following realistic perturbations of the data:

- First, the highly resolved reference solution was subsampled on grids with element spacing of 0.1, 0.15, 0.2 and 0.25 cm.
- Then, it was subsampled in time at 0.02 s.
- Finally, an additive Gaussian noise was added to the subsampled velocity at each mesh node and for each time. The standard deviation chosen as 10% of the peak velocity for all velocity components as it is usually done in clinical Phase-Contrast imaging adjusting the expected peak velocity (called *VENC* parameter) [4].

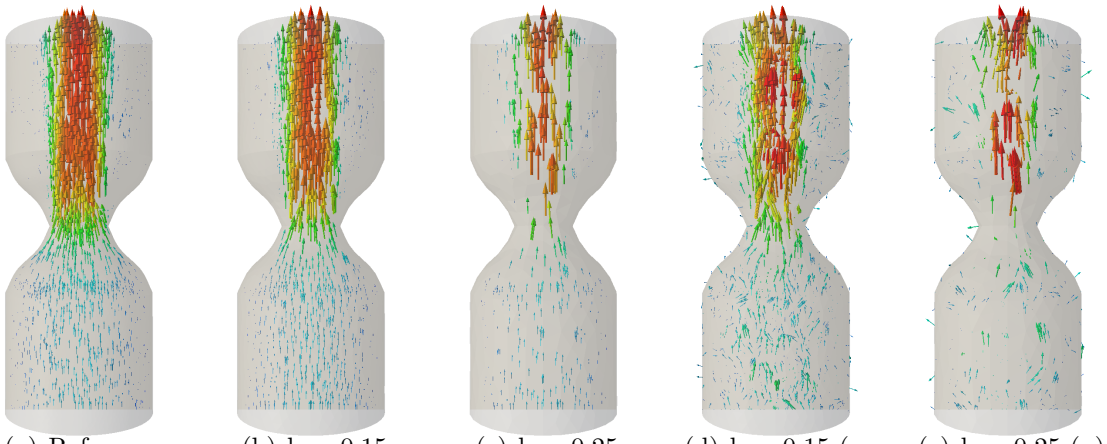

(a) Reference (b) h = 0.15 (c) h = 0.25 (d) h = 0.15 (n (e) h = 0.25 (n)

Figure 2: (a)Reference simulated velocity field (with $h = 0.06$ cm and mini-elements). (b)-(c) Spatially subsampled measurements at time $t = 0.25$ s (noise free). (d)-(e) Spatially subsampled and noisy (n) measurements at time $t = 0.25$.

6.3 Weighting functions for IMRP

We will use a Poiseuille flow as test functions $\boldsymbol{v}$ for the IMRP method, which can be appreciated in Figure 3.

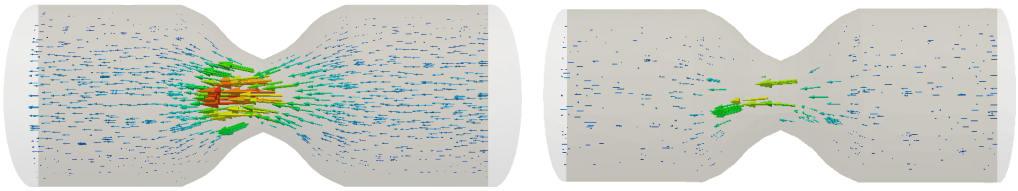

(a) $h = 0.15$ cm (b) $h = 0.25$ cm

Figure 3: Poiseuille test functions for IMRP for different spatial resolutions.

We remark that this is not the only possible choice for $\boldsymbol{v}$. Alternatives may be Brinkman or Darcy flows. Nevertheless, In several numerical test that we performed no advantage over a simple Poiseuille flow was established in the pressure gradient results. Specifically, the results of the Brinkman flow were dependent on the weighting of the mass term, possibly leading to deteriorated results if this weight was chosen either too large or too small. In the case of a Darcy flow, this is in fact a naive choice due to the lack of regularity of the solutions gradient, which is need in the evaluation of the IMRP in Equation (18). A further option would be to include convective terms for $\boldsymbol{v}$, but this leads to considerably worse approximation results of the IMRP. Therefore, we do not present any results for these alternative test functions for the sake of clarity and conciseness.

6.4 Bias of the estimators

As we remarked in Section 5, we can compute a priori the bias for all methods, which are shown in Table 1. Only in the case of the WERP, the bias coming from the convective term needs to be computed from the ground truth. However, we show that for small mesh spacing the bias of the WERP is dominated by the viscous part, which is again independent on the ground truth velocity field, see Equation (30).

For this example, the bias for the STE, STEint and DAE are of the order of the machine precision. The bias of the PPE is also very small. The IMRP turns to give a negligible bias.

h [cm]	0.1	0.15	0.2	0.25
PPE	$5.7e-13$	$2.1e-13$	$1.4e-13$	$1.0e-13$
STE	$-1.6e-16$	$-1.0e-16$	$-1.6e-16$	$-1.6e-16$
STEint	$1.0e-17$	$8.6e-17$	$7.8e-17$	$-2.4e-17$
DAE	$3.3e-17$	$1.7e-16$	$7.0e-17$	$-9.6e-18$
WERP	2.3	0.9	0.6	0.5
WERP(visc)	2.3	1.0	0.3	1.1
IMRP	$4.2e-06$	$-5.1e-06$	$-7.9e-06$	$-4.1e-08$

Table 1: Computation of the estimators bias [mmHg] for 10% noise in the velocity.

6.5 Estimation results: noise-free measurements

We first study the sensitivity of the relative pressure estimation to spatial subsampling of the measurements, without any random noise. The results are shown in Figure 4, and the error convergence curves with respect to the data resolution h are shown in Figure 5. Note that the best methods turn out finally to be the IMRP and STEint, with the former giving a slightly better precision. They turn out to be more robust when subsampling the measurements compared with the state of the art methods, i.e. PPE, STE and WERP. Note that the PPE, which is the oldest and the most spread approach, was consistently the worst method, in line with the findings of [10, 3]. We also remark that the temporal subsampling at this realistic level does not have a considerable impact on the estimation precision, compared with the space subsampling, and hence only the time-subsampled results are shown for the sake of conciseness.

6.6 Estimation results: noisy measurements

Now we summarize the results with noisy measurements, for which we consider 100 random realizations of the noise $\boldsymbol{\varepsilon}^n$ for each n. The standard deviations of the relative pressure estimation and the error of the mean with respect to the ground truth (both at peak systole) are presented in Figure 6 and 7. Note that both diminish with the spatial discretization size h for all methods. In addition, by comparing Figures 4 and 6 we verify

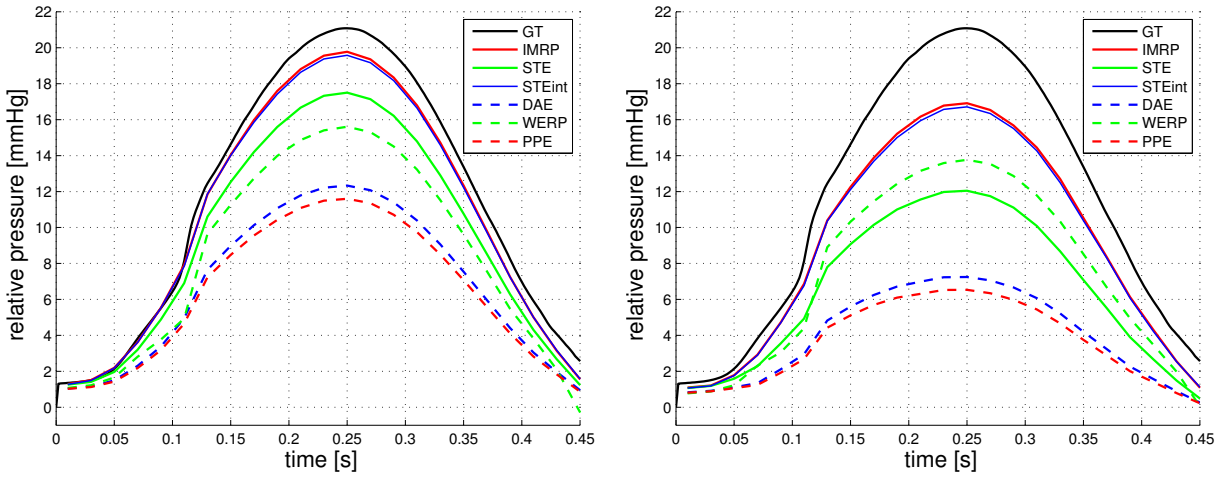

(a) $h = 0.15$ cm (b) $h = 0.25$ cm

Figure 4: Reference ground-truth (GT) and noise-free relative pressure estimations for two different spatial subsampling resolutions including temporal subsampling of 0.02 s.

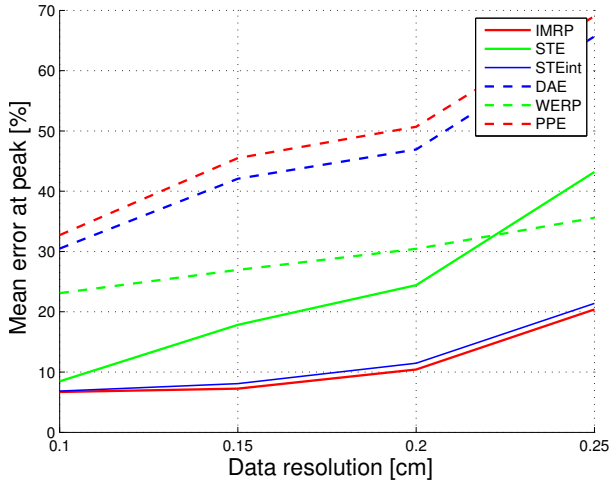

Figure 5: Error of estimation with respect to the ground truth at peak systole for noise-free but spatial subsampled measurements.

that the bias is imperceptible, consistently with the values computed a priori in Table 1. Also consistent with Table 1, the only exception is the WERP.

As expected due to the "squaring" of the measurements, the method with highest variance is the WERP, while the methods delivering sharper standard deviations are PPE and DAE. However, the differences in standard deviations among all methods are around 1.0 mmHg, meaning around 2.0 mmHg for a 95% confidence interval.

In summary, these results confirm that the best performing methods (also when including noise and subsampling) are the IMRP and the STEint.

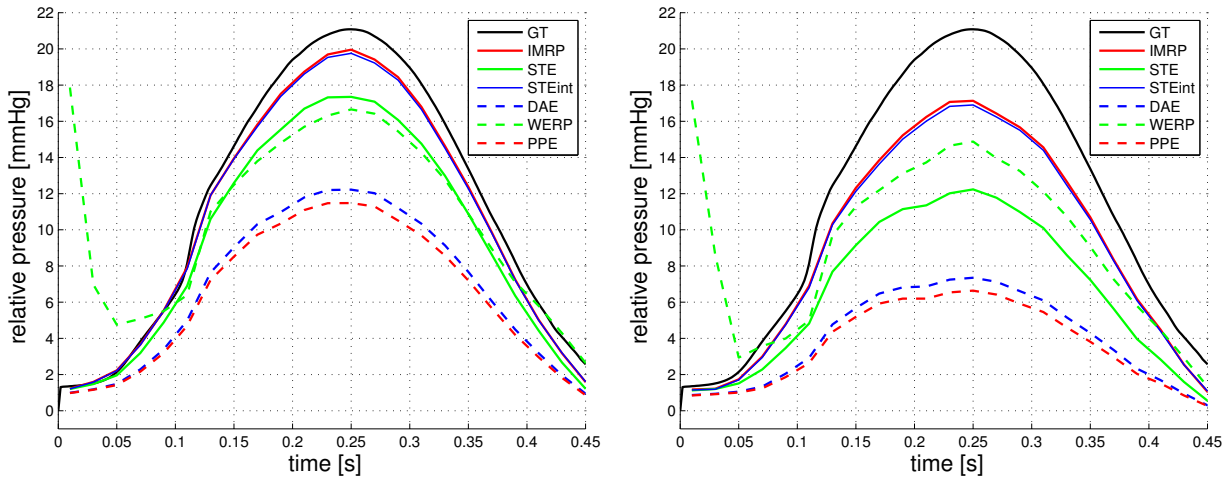

(a) $h = 0.15$ cm (b) $h = 0.25$ cm

Figure 6: Mean pressure estimations with noisy measurements.

7 Conclusions

In this work we reviewed, improved, analyzed (both theoretically and numerically) and compared old and recent approaches for estimating relatives pressures from 4D flow data. Consistent with recent findings, the worst performance was found the be of the widely spread PPE method in terms of its robustness the spatial subsampling.

The WERP method recently introduced in [3], while being the computationally cheapest, it is more sensitive to noise, delivering biased estimations and larger variances than the other methods. The bias of the WERP at higher data resolutions is controlled by the viscous term. However, in our specific numerical test, this term is anyway negligible with respect to the convective one, so it could be neglected from the WERP formulation, avoiding biasing.

We also performed computations for the STE method also recently introduced in [10], confirming that it performs better than the PPE. However, it also presented an important sensitivity when the measurements are subsampled in space. We found out that just a simple integration by parts, in particular of the convective term, considerably reduces this

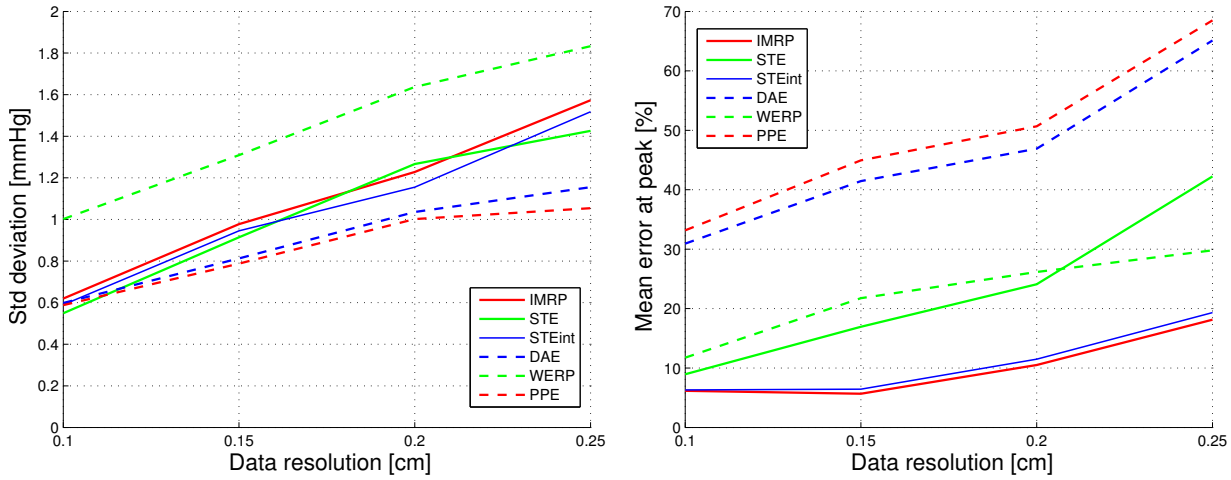

(a) Standard deviation

(b) Mean error

Figure 7: Estimation results at peak systole with noisy measurements.

sensitivity, and we called it STEint. This was not shown in the original article [10]. In this context, we investigated an alternative to the STE method based on the Darcy flow, which we called DAE, obtaining slightly better results than the PPE but worse than the rest of the approaches in terms of estimated mean.

Finally, inspired from the integral approach introduced by the WERP, we proposed a new method based on an integral momentum balance weighted by a simple Poiseuille solution. This turns out to be the most accurate method together with the STEint, with a low sensitivity to spatial subsampling in current clinical ranges of voxel size used for 4D flow acquisitions.

Summarizing, based on the numerical experiments presented in this work, the methods of choice would be the IMRP and/or the STEint, both newly introduced in our contribution. While the STEint has the advantage of given the full spatial distribution of the pressure (relative to some point), the IMRP is computationally cheaper when the relative pressure needs to be computed at many time frames. Therefore, future work will consist on further comparing and validating these approaches using real 4D flow data and catheter measurements.

Acknowledgements

We sincerely thank discussions with Alfonso Caiazzo and Alexander Linke from WIAS Berlin about finite element discretizations, and with Sergio Uribe and Joaquín Mura from the Center for Biomedical Imaging of the Universidad Católica de Chile about Phase-Contrast MRI. D. Nordsletten acknowledges funding from BHF New Horizons program (NH/11/5/29058) and the Engineering and Physical Sciences Research Council (EP/N011554/1).

The rest of the authors sincerely thank the Conicyt Basal Program PFB-03 for its support.

References

[1] Cristóbal Bertoglio and Alfonso Caiazzo. A Stokes-residual backflow stabilization method applied to physiological flows. *Journal of Computational Physics*, 313:260–278, 2016.

[2] Alexander N Brooks and Thomas JR Hughes. Streamline upwind/Petrov-Galerkin formulations for convection dominated flows with particular emphasis on the incompressible Navier-Stokes equations. *Computer methods in applied mechanics and engineering*, 32(1):199–259, 1982.

[3] Fabrizio Donati, C Alberto Figueroa, Nicolas P Smith, Pablo Lamata, and David A Nordsletten. Non-invasive pressure difference estimation from PC-MRI using the work-energy equation. *Medical Image Analysis*, 26(1):159–172, 2015.

[4] Petter Dyverfeldt, Malenka Bissell, Alex J Barker, Ann F Bolger, Carl-Johan Carlhäll, Tino Ebbers, Christopher J Francios, Alex Frydrychowicz, Julia Geiger, Daniel Giese, et al. 4D flow cardiovascular magnetic resonance consensus statement. *Journal of Cardiovascular Magnetic Resonance*, 17(1):1–19, 2015.

[5] Tino Ebbers and Gunnar Farnebäck. Improving computation of cardiovascular relative pressure fields from velocity MRI. *Journal of Magnetic Resonance Imaging*, 30(1):54–61, 2009.

[6] Tino Ebbers, Lars Wigström, Ann F Bolger, Jan Engvall, and Matts Karlsson. Estimation of relative cardiovascular pressures using time-resolved three-dimensional phase contrast MRI. *Magnetic resonance in medicine*, 45(5):872–879, 2001.

[7] Sebastian BS Krittian, Pablo Lamata, Christian Michler, David A Nordsletten, Jelena Bock, Chris P Bradley, Alex Pitcher, Philip J Kilner, Michael Markl, and Nic P Smith. A finite-element approach to the direct computation of relative cardiovascular pressure from time-resolved MR velocity data. *Medical image analysis*, 16(5):1029–1037, 2012.

[8] Pablo Lamata, Alex Pitcher, Sebastian Krittian, David Nordsletten, Malenka M Bissell, Thomas Cassar, Alex J Barker, Michael Markl, Stefan Neubauer, and Nicolas P Smith. Aortic relative pressure components derived from four-dimensional flow cardiovascular magnetic resonance. *Magnetic resonance in medicine*, 72(4):1162–1169, 2014.

[9] Michael Markl, Alex Frydrychowicz, Sebastian Kozerke, Mike Hope, and Oliver Wieben. 4D flow MRI. *Journal of Magnetic Resonance Imaging*, 36(5):1015–1036, 2012.

[10] H Švihlová, J Hron, J Málek, KR Rajagopal, and K Rajagopal. Determination of pressure data from velocity data with a view toward its application in cardiovascular

mechanics. Part 1. Theoretical considerations. *International Journal of Engineering Science*, 2016, In press.

[11] Roger Temam. Une méthode d'approximation de la solution des équations de navier-stokes. *Bulletin de la Société Mathématique de France*, 96:115–152, 1968.

[12] Alec Vahanian, Ottavio Alfieri, Felicita Andreotti, Manuel J. Antunes, Gonzalo Barón-Esquivias, Helmut Baumgartner, Michael Andrew Borger, Thierry P. Carrel, Michele De Bonis, Arturo Evangelista, Volkmar Falk, Bernard Iung, Patrizio Lancellotti, Luc Pierard, Susanna Price, Hans-Joachim Schäfers, Gerhard Schuler, Janina Stepinska, Karl Swedberg, Johanna Takkenberg, Ulrich Otto Von Oppell, Stephan Windecker, Jose Luis Zamorano, Marian Zembala, , Jeroen J. Bax, Helmut Baumgartner, Claudio Ceconi, Veronica Dean, Christi Deaton, Robert Fagard, Christian Funck-Brentano, David Hasdai, Arno Hoes, Paulus Kirchhof, Juhani Knuuti, Philippe Kolh, Theresa McDonagh, Cyril Moulin, Bogdan A. Popescu, Željko Reiner, Udo Sechtem, Per Anton Sirnes, Michal Tendera, Adam Torbicki, Alec Vahanian, Stephan Windecker, , Bogdan A. Popescu, Ludwig Von Segesser, Luigi P. Badano, Matjaž Bunc, Marc J. Claeys, Niksa Drinkovic, Gerasimos Filippatos, Gilbert Habib, A. Pieter Kappetein, Roland Kassab, Gregory Y.H. Lip, Neil Moat, Georg Nickenig, Catherine M. Otto, John Pepper, Nicolo Piazza, Petronella G. Pieper, Raphael Rosenhek, Naltin Shuka, Ehud Schwammenthal, Juerg Schwitter, Pilar Tornos Mas, Pedro T. Trindade, and Thomas Walther. Guidelines on the management of valvular heart disease (version 2012). *European Heart Journal*, 33(19):2451–2496, 2012.

[13] C.A. Warnes, R.G. Williams, T.M. Bashore, J.S. Child, H.M. Connolly, J.A. Dearani, P. del Nido, J.W. Fasules, T.P. Graham, Z.M. Hijazi, S.A. Hunt, M.E. King, M.J. Landzberg, P.D. Miner, M.J. Radford, E.P. Walsh, and G.D. Webb. ACC/AHA 2008 Guidelines for the Management of Adults with Congenital Heart Disease: a report of the American College of Cardiology/American Heart Association Task Force on Practice Guidelines (writing committee to develop guidelines on the management of adults with congenital heart disease). *Circulation*, 118(1):714–833, 2008.

[14] Carole A Warnes, Roberta G Williams, Thomas M Bashore, John S Child, Heidi M Connolly, Joseph A Dearani, Pedro del Nido, James W Fasules, Thomas P Graham, Ziyad M Hijazi, et al. ACC/AHA 2008 guidelines for the management of adults with congenital heart disease. *Journal of the American College of Cardiology*, 52(23):e143–e263, 2008.